# Substitutional Boron in Nanodiamond, Bucky-Diamond, and Nanocrystalline Diamond Grain Boundaries

**A. S. Barnard*,† and M. Sternberg‡**

*Department of Materials, University of Oxford, Parks Road, Oxford OX1 3PH, United Kingdom, and Center for Nanoscale Materials, Argonne National Laboratory, 9700 South Cass Avenue, Argonne, Illinois 60439*

*Received: June 2, 2006; In Final Form: August 1, 2006*

Although boron has been known for many years to be a successful dopant in bulk diamond, efficient doping of nanocrystalline diamond with boron is still being developed. In general, the location, configuration, and bonding structure of boron in nanodiamond is still unknown, including the fundamental question of whether it is located within grains or grain boundaries of thin films and whether it is within the core or at the surface of nanoparticles. Presented here are density functional tight-binding simulations examining the configuration, potential energy surface, and electronic charge of substitutional boron in various types of nanocrystalline diamond. The results predict that boron is likely to be positioned at the surface of isolated particles and at the grain boundary of thin-film samples.

## 1. Introduction

For electronic applications, the common objective in the doping of diamond is the production of *p*-type and *n*-type semiconductors materials. Boron (incorporated substitutionally via replacement of a carbon atom) is currently the most successful and widely used acceptor in diamond, introduced both during CVD diamond film growth[1,2] and by ionimplantation[3] as well as via forced diffusion.[3] With the advent of nanocrystalline diamond thin films[4−9] with grain sizes in the order of ∼5−50 nm (depending upon growth conditions), there has been growing interest in the doping of such materials for electronic purposes. The success of such doping will be largely dependent upon the positions of the dopants within the films and the nature of the bonding of the dopant atoms to the surrounding carbon atoms. While computational studies investigating the configuration and bonding of boron within the nanocrystalline diamond films could not be found, some studies of boron in nanocrystalline diamond thin films have been undertaken using experimental methods.[10−13]

Transmission electron spectroscopy has been used by Yater et al. to examine the low-energy electron transport and emission properties[10] and the effect of transport distance, diamond nanostructure, and electron affinity on the cold emission characteristics of boron-doped nanocrystalline diamond films. Particular attention was given to the intensity and energy distribution of transmitted electrons measured as a function of film thickness,[10,11] surface properties,[11] and incident-beam parameters.[10] The transmitted energy distributions were found to be similar for two films of thicknesses 0.15 and 2.5 $\mu$m (with similar boron concentrations) and were in good agreement with results obtained in reflection measurements. The energy-dependent data was interpreted using Monte Carlo simulations along with a qualitative model of the diamond nanostructure.[10,11] The deposition, characterization, and electrochemical responsiveness of boron-doped nanocrystalline diamond thin-film electrodes was reported by Show et al.[13] The films consist of 50−100 nm clusters composed of 10−15 nm grains. The films were characterized by scanning electron microscopy, atomic-force microscopy, transmission electron microscopy, visible-Raman spectroscopy, X-ray diffraction, boron-nuclear-reaction analysis, and cyclic voltammetry. The electrical properties investigated during this study were found to be dominated by charge carriers in the grains,[13] and it was concluded that the dopants are positioned within the diamond lattice of the grains rather than at the grain boundary. However, it is not clear from these results how the exposure of surface grain boundary structure by plasma treatment (resulting in a type of porosity) may play a role. More recently, Lee et al.[14] have studied the effect of boron doping on the electron-field-emission properties of nanodiamond films, and Cheng et al.[15] examined boron-doped nanodiamond films using current image tunneling spectroscopy. Unfortunately, in each of these studies, the nature of the bonding and effects of the boron atoms on the local structure were not explicitly examined.

The case of particulate nanodiamond produced using detonation synthesis, often referred to as detonation nanodiamond or ultradispersed diamond (UDD), is somewhat different. Detonation nanodiamonds are usually around ∼2−6 nm in diameter, with either a hydrogenated surface or a fullerenic outer shell (then denoted as "bucky-diamond"). In addition to possible nanoscale electronic applications, the study of dopants and impurities in particulate nanodiamond is also considered important because doped nanodiamonds have been suggested as candidates for use as qubits for quantum computing.[16] The main objective in this case is to find "stable" dopants with suitable spin states, but before the electronic or spin properties of impurities in nanodiamond may be examined, it is first important to establish which dopant species may be expected to be stable at given sites within the nanodiamond lattice. For a dopant in nanodiamond to be considered stable in this context,[16] it must be included substitutionally and it must exhibit negligible diffusion to the nanocrystallite surface. It should be pointed out that the stable incorporation of boron into these

* Corresponding author. E-mail: amanda.barnard@materials.ox.ac.uk.
† Department of Materials, University of Oxford.
‡ Center for Nanoscale Materials, Argonne National Laboratory.

10.1021/jp0634252 CCC: $33.50 
Published on Web 09/07/2006

particles (experimentally) has not yet been reported, making a fundamental knowledge of the stability of these systems critical to guide further development.

To address these questions, we employ density functional tight-binding calculations to determine the configuration, energetics, and charge distribution of substitutional boron in model nanocrystalline diamond films as well as bucky-diamond and nanodiamond particles. The results predict that it is energetically preferable for boron to be positioned just beneath the surface of nanodiamond and bucky-diamond and within the grain boundaries of thin films. The present study has also been designed to complement our previous work on the structure and stability of nitrogen in nanodiamond and bucky-diamond particles, and comparisons will be drawn between the two where appropriate.

## 2. Computational Methods

The density-functional-based tight-binding method with self-consistent charges (SCC-DFTB)[17,18] is a two-center approach to density functional theory (DFT). In short, the Kohn−Sham density functional is expanded to second order around a reference electron density. The reference density is obtained from self-consistent density functional calculations of weakly confined neutral atoms within the generalized gradient approximation (GGA). The confinement potential is optimized to anticipate the charge density and effective potential in molecules and solids. A minimal valence basis is established, and one- and two-center tight-binding matrix elements are calculated (rather than fitted) within DFT. A universal short-range repulsive potential accounts for double-counting terms in the Coulomb and exchange-correlation contributions as well as the internuclear repulsion. Self-consistency is included at the level of Mulliken charges.

This method has been selected for use here as it has previously been shown to provide good agreement with higher-level quantum chemical methods for all-carbon and carbon−nitrogen systems (such as the interaction of CN with diamond surfaces[19]), and it has proven very successful in modeling the inclusion of nitrogen in nanodiamond and bucky-diamond[20] as well as nanocrystalline diamond grain boundaries.[21]

## 3. Discussion of Results

We used this technique to model the substitutional boron in the grain and grain boundary (GB) of nanocrystalline diamond thin films and in isolated bucky-diamond and nanodiamond particles. All structures were first fully prerelaxed using the conjugate gradient scheme to minimize the total energy. The convergence criterion for a stationary point is $10^{-4}$ a.u. $\approx$ 5 meV/Å for atomic forces.

The grain boundary structure studied is a $\Sigma 13$ − (001) twist grain boundary, similar to the models studied in ref 21, and is illustrated in Figure 1a. Briefly, this model is constructed from a coincident site-lattice model with a square lateral unit cell along [230] and consequently containing 13 atoms per monolayer. The vertical extent of the cell is 12 monolayers along [001], half of which are taken along the conjugate [$\bar{2}$30] direction. This results in two grain boundaries, each with a twist angle of 67.4° (see also Figure 2). The resulting supercell was optimized following a simulated annealing procedure. A free-volume correction along the twist axis was allowed, which resulted in an expansion of the supercell along the twist axis by 0.50 Å per GB. The undoped grain boundary structure has been discussed in detail in ref 21. Two key points are that disorder is limited to the two monolayers constituting each grain boundary and that among the atoms in these layers, approximately 50% are 3-fold coordinated.

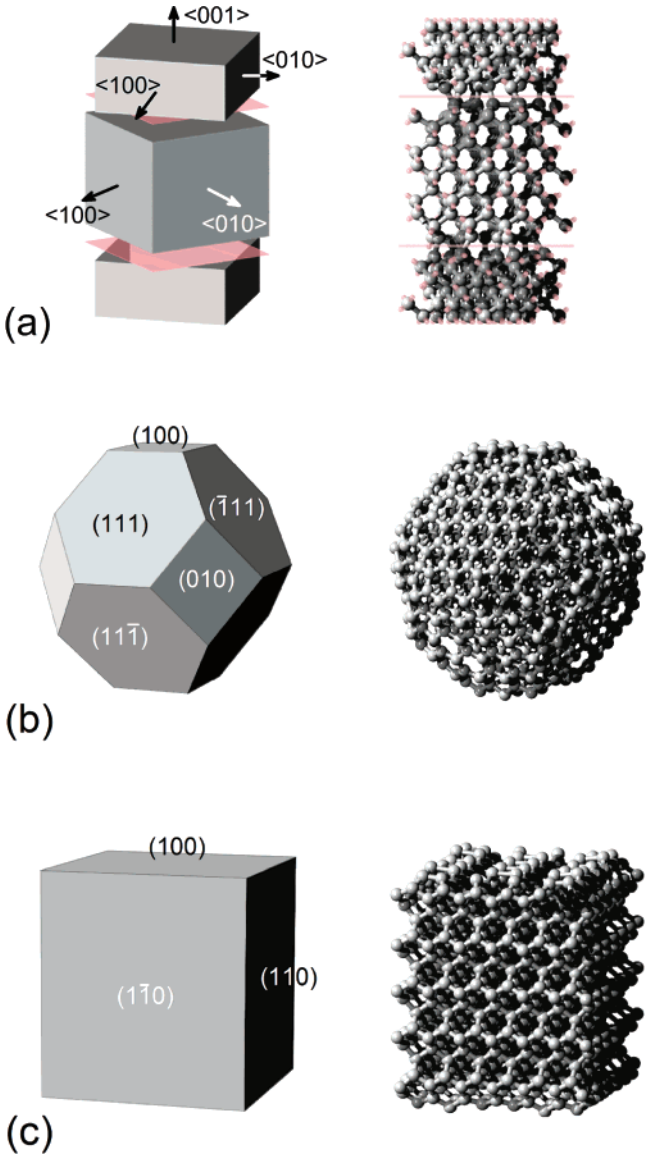


**Figure 1.** Schematic (left) and structural (right) representations of (a) the nanocrystalline diamond thin-film grain and grain boundary, (b) the bucky-diamond, and (c) the nanodiamond particles. The planes and terminal "sticks" in (a) indicate the plane of the grain boundary and the position of the periodic directions, respectively.

In addition to this, two isolated nanoparticle structures were constructed, consisting of 837 and 881 carbon atoms, with a truncated-octahedral and cubic morphologies (as illustrated in Figure 1b and c), respectively. These particles measure ~2.2 nm in diameter, a size (within the nanodiamond "window" of stability[22]) that occupies the boundary of stability for bucky-diamond and dehydrogenated nanodiamond.[23] The $C_{837}$ truncated-octahedral structure exhibited delamination of the {111} surfaces and {111}/{111} edges upon relaxation, thereby becoming a bucky-diamond, as shown in Figure 1b. The outer surface/shell remained anchored to the core along {111}/{100} edges, and the {100} surfaces reconstructed to form the (2 × 1) surface structure, in full agreement with results of previous studies obtained using first principles methods.[24] The $C_{881}$ cubic nanodiamond particle retained the diamond structure upon relaxation, with the {100} surfaces relaxing to form the (2 × 1) reconstruction, as shown in Figure 1c, in agreement with first principles results for nanodiamonds of this shape.[25] An

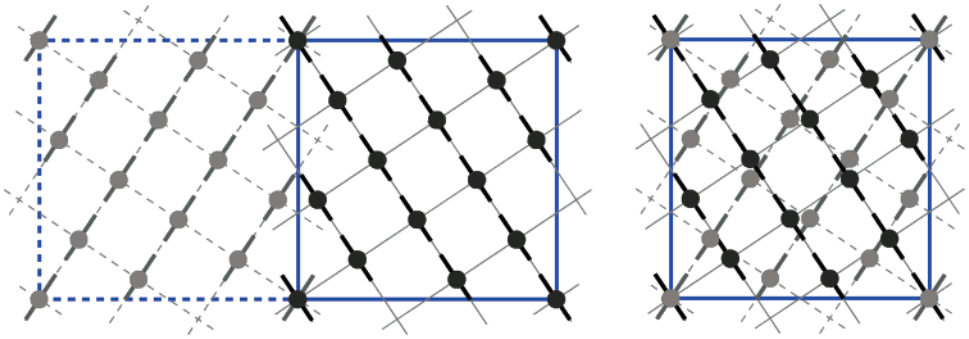

**Figure 2.** Schematic representations illustrating the orientation of the $\Sigma 13-(001)$ twist grain boundary, constructed from a coincident site-lattice model with a square lateral unit cell, half along the [230] direction (far left), and half along the conjugate [$\bar{2}$30] direction (center left). The overlap results in a grain boundary (right) with a twist of 67.4°.

interesting feature of this particle is the effect of surface reconstructions on the overall (relaxed) shape. The flattening of the {110} surfaces (as a result of the relaxation) induces a slight concave curvature on the {100} surfaces (perpendicular to the (2 × 1) dimer rows). In addition, the {100} (2 × 1) dimers at each end of the center row open up due to a combination of stress and charge redistribution at the edge. Although quite unusual, and unexpected, this dimer opening involves the breaking of the (2 × 1) bond (with a final separation distance of ∼3 Å) and the terminal atoms bending away from one another with an angle of ∼79° between them. The charge distribution will be shown in more detail in Section 3.5. The dimers on the {100} surfaces also vary in length and tilt angle, depending upon location (with respect to corners and edges), but are symmetric across the facets. More details on the reconstruction of this (undoped) structure will be given in a future publication.

The fully relaxed structures were then used as initial configurations for subsequent calculations involving the inclusion of boron dopants. In all cases, single boron atoms were substituted for carbon atoms located along specific substitution paths within the lattices.[26] For the GB model, the substitution paths are shown in Figure 3a. The main path traverses a grain from one boundary to the other, principally following the direction of the [001] twist axis and fanning out at both ends. The essential spatial parameter for the paths is the distance from the grain center. The paths are denoted as 1 and 2 within the two halves of the grain. Paths 1a−1c terminate within the GB layer itself and differ by their end atom, with path 1c having a distinct second-layer atom as well. Paths 2a and 2b terminate on the other side of the grain at the sub-GB layer at two distinct sites. All end sites were chosen to be representative of carbon atoms in the various coordination and bond angle configurations encountered in the disordered GB layers.

In the isolated particles, the substitution paths extend from the centrosymmetric atom to different points on the surface. The directions of the substitution paths in the bucky-diamond are shown in Figure 3b, denoted as A1, B, C, D, and E for paths terminating at the center of the {100} surface, {111} surface, {100}/{111} edge, {111}/{111} edge, and the {100}/{111}/{111} corner, respectively. These are the same substitution paths examined for nitrogen dopants in ref 20. The directions of the substitution paths in the nanodiamond are shown in Figure 3c, denoted as A2, F, G, H, and I for paths terminating at the center of the {100} surface, {110} surface, {100}/{110} edge, {110}/{110} edge, and the {100}/{110}/{110} corner, respectively. This choice of paths has two main advantages. First, they allow for direct comparison of nine distinct crystallographic directions and extremum sites, and

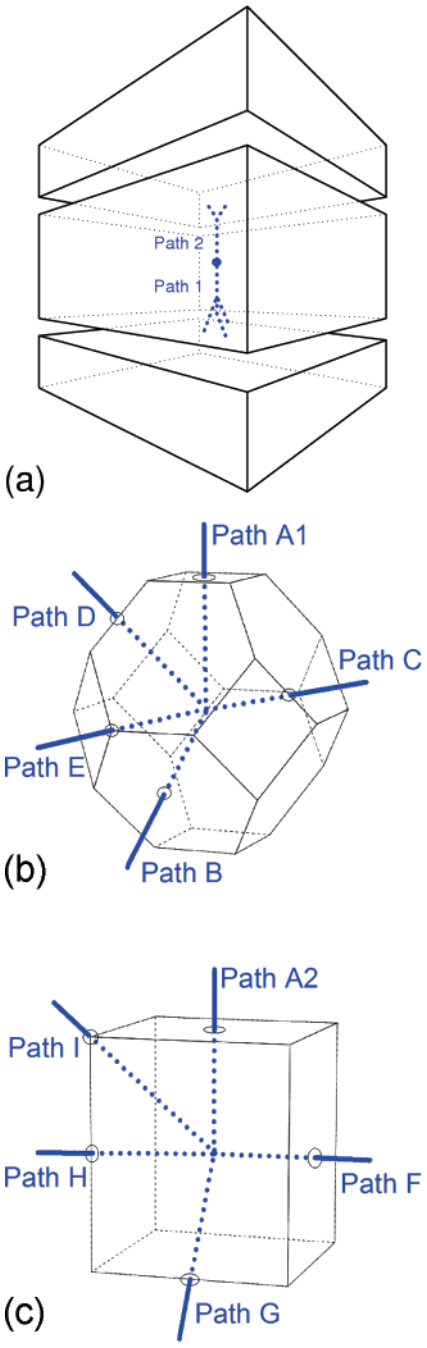


**Figure 3.** A schematic representation of the substitution paths examined in (a) the nanocrystalline diamond thin-film grain and grain boundary, (b) the bucky-diamond, and (c) the nanodiamond particles.

second, they facilitate the investigation of how the shape of the nanoparticle can affect the potential energy surface by allowing direct comparison of the same path and sites (A1 and A2) in both truncated-octahedral and cubic structures.

At each lattice site along the substitution paths, the boron dopant and the first- and second-nearest neighboring carbon atoms were re-relaxed, again to a force convergence of $10^{-4}$ a.u. In a previous study,[20] we have explicitly validated this "second-nearest neighbor relaxation" for the case of nitrogen and have shown that re-relaxing two neighbor shells is sufficient to model the configuration and energetic of dopants in diamond at the nanoscale. Like nitrogen, the results of previous first principle studies[27] have shown that the disruptive influence of boron within the diamond lattice is localized so it has been assumed here that our previous tests will also apply in this case.

In the following sections, the structure and energetics of the boron along each of these substitution paths are compared, and the energetically preferred location and configuration of boron for each type of nanocrystalline diamond is identified. This is followed by an analysis of the charge distribution surrounding these sites in each structure.

**3.1. Nanocrystalline Diamond Films.** Upon boron substitution of carbon sites in the GB model, the coordination is unchanged at most sites. For all sites in the grain interior, which essentially represents bulk diamond, the coordination is 4-fold tetrahedral with an outward relaxation of approximately 4%. This is slightly larger than first principle results by Goss et al.,[28,29] where $C_{3v}$ symmetry with approximately a 2% extension for the 3-fold neighors is reported. Lombardi et al.,[30] using the same method on a $BC_{164}H_n$ cluster, report a $C_{3v}$ defect structure with a much larger extension of 18%, but point to the possibility of $T_d$ structures as well.[31]

For carbon sites at the grain boundary layer, the coordination is also maintained, although we note slightly larger displacements of about 0.2 Å, facilitated by the free volume and disorder at the GB. As indicated previously, these results stem from relaxations of atoms up to the second-nearest neighbor. We have performed additional relaxations where all atoms were allowed to move. Those led to essentially the same results with the exception of GB sites, where we observed coordination changes in a few cases. To ensure that all local structural changes can reliably be attributed to the inclusion of the B atom, we consider only results from the constrained relaxations.

The substitution energy as a function of position within the grain is shown in Figure 4a. Here, the *x*-axis represents a scaled (dimensionless) distance obtained by dividing the distance from the monolayer at the center of the central "grain" to the dopant site ($r_X$), by the total distance from the center to the GB ($R_X$) in the corresponding direction ($X = 1$ or 2). The energy $E - E_{\text{center}}$ is given as the total energy for each substitutional site relative to the total energy of the system with the dopant in the center of the "grain". As we can see from Figure 4a, the energy is within 1 eV of the center site for all bulk-like sites. For the majority of sites in the immediate GB layer and its adjacent monolayer, the energy is 2−2.5 eV lower than at the center. The most stable site is the endpoint of 1c, where both the original carbon and (after substitution) the boron atom is in 3-fold planar configuration within the GB layer. The second-most stable site is the endpoint of path 2a and lies at 2.2 eV below the center site. The site forms the pedestal of a (2 × 1)-like intragrain-boundary dimer and as such is structurally and energetically similar to a subsurface site for path A1, as discussed below in Section 3.2 and is evident from Figure 4b. The end site of path 2b is higher in energy than that of 2a. We note here the overall largest relaxation of a second-neighbor atom (by about 0.15 Å), indicative of a somewhat higher local strain, as can be expected given the disordered GB structure. Overall, a comparison of all substitution sites chosen within the GB indicates that boron is preferentially located near the grain boundaries.

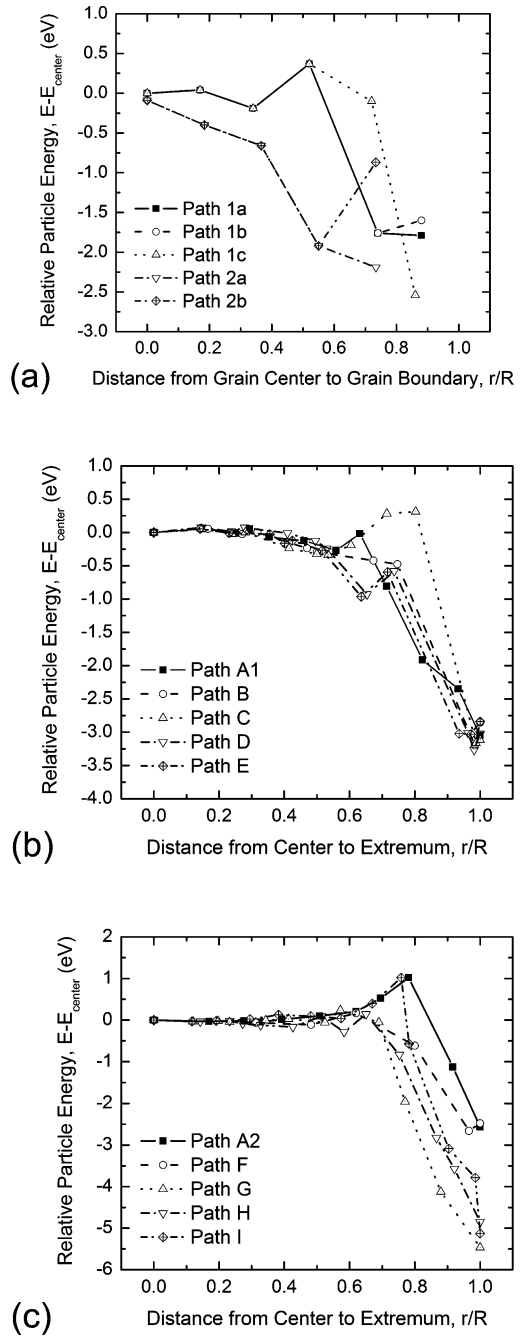


**Figure 4.** The relative nanoparticle energy $E - E_{\text{center}}$ for each substitutional site of the B atom in (a) the nanocrystalline diamond thin-film grain and grain boundary, (b) the bucky-diamond, and (c) the nanodiamond particles. The dimensionless nanoparticle distance $r/R$ is obtained by dividing the distance from the center of each structure to the substitution site by the total distance from the center to the extremum (for each direction). Hence $r/R = 0$ is the center and $r/R = 1$ is the outermost substitution site located on an extremum (for each substitution path).

This result seems at odds with the experimental findings of Show et al.[13] mentioned above, where boron was predicted within the grain. There are two possible explanations for this incongruence. First, that the boron is trapped within the grains

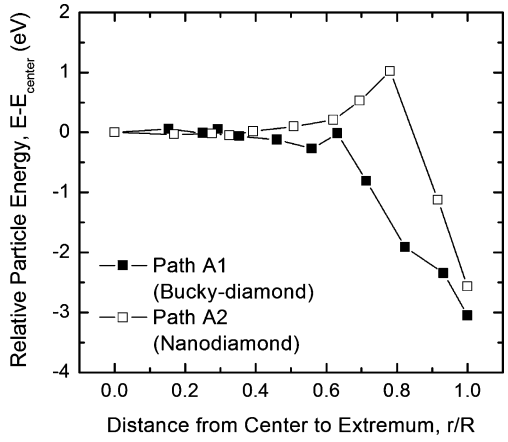


**Figure 5.** The relative nanoparticle energy $E - E_{center}$ for each substitutional site along the {100} direction for the B atom in the bucky-diamond (A1) and the nanodiamond (A2) particles. Because this surface does not delaminate in the bucky-diamond structure, the difference in energy of these paths is attributed to the different nanoparticles shapes.

**TABLE 1: Net Mulliken Charges for the Extremum and Central Substitutional Sites in the Undoped and Doped Grain Boundaries, Bucky-Diamonds, and Nanodiamond Nanoparticles**[a]

| | net charge | | |
|---|---|---|---|
| site | C | B | (B−C) |
| 1a | −0.01 | −0.09 | −0.08 |
| 1b | −0.02 | −0.15 | −0.14 |
| 1c | −0.07 | 0.18 | 0.25 |
| center | 0.00 | −0.20 | −0.20 |
| 2a | −0.08 | −0.06 | 0.02 |
| 2b | 0.01 | −0.01 | −0.02 |
| A1 | −0.96 | 0.07 | 1.03 |
| B | 0.22 | 0.05 | −0.18 |
| C | −0.99 | −0.19 | 0.79 |
| D | −0.34 | −0.06 | 0.29 |
| E | −0.52 | −0.98 | −0.47 |
| center | 0.01 | −0.29 | −0.31 |
| A2 | −1.02 | 0.08 | 1.10 |
| F | 0.26 | 0.10 | −0.15 |
| G | 0.13 | 0.35 | 0.21 |
| H | −0.18 | −0.24 | −0.06 |
| I | −0.30 | −0.36 | −0.07 |
| center | 0.00 | −0.30 | −0.31 |

[a] Last Column Gives the Difference.

kinetically during growth and the energetic barrier is too high to facilitate diffusion to the grain boundary, and second, that the theoretical result presented are influenced by the limits imposed by the second-nearest neighbor approximation. As stated above, we have systematically compared results both with and without this approximation (finding little difference) and must conclude that the second explanation appears unlikely.

**3.2. Bucky-Diamond.** In the case of bucky-diamond, the coordination of boron atoms was found to be insensitive to the substitution path, preferring 4-fold coordination throughout the core of the particle (right out to the subsurface sites). At the substitution sites at the extremum (of each path), and in some cases the subsurface sites, the boron atoms were also found to be stable in the (natural) 3-fold coordinated sites. Although (in most cases) the boron atoms near the extremum exhibited quite significant outward displacements, in only three instances did the boron atoms adopt a different coordination than the carbon atom they replaced. The boron atom located on the "inner surface" of a bucky-diamond core along path B reattached to the shell (changing from 3-fold to 4-fold coordination during the relaxation), and the boron atoms occupying the subextremum sites in paths C and E broke bonds with the more corelike C neighbors (changing from 4-fold to 3-fold coordination).

In addition to the general decrease in energy as the boron substitution sites neared the extremum, the energetic results show a number of features indicating a dependence on substitution path. These results are shown in Figure 4b, where the *x*-axis is a scaled nanoparticle radius obtained by dividing the distance from the center to the substitution site ($r_X$) by the total distance from the center to the extremum ($R_X$) in the corresponding direction ($X$). Hence, in these structures $r/R = 0$ is the center, and $r/R = 1$ is the outermost substitution site located on an extremum (surface, edge, or corner). Similarly, $E - E_{center}$ is given as the total energy for each substitutional site relative to the total energy of the nanoparticles with the boron atom in the centrosymmetric position.

We can see that near the core, at less than $r/R \approx 0.5$ in Figure 4b, the results are insensitive to the substitution path,[32] but beyond this range (as the sites approach in the "inner surface" of the bucky-diamond core), differences begin to emerge. Paths A1 and C (towards the {100} surface and {100}/{111} edge) show a sharp increase of ∼0.25 eV in energy at $r/R \approx 0.6$. This increase continues (a further ∼0.25 eV) for path C, making this substitution site endothermal, but sharply decreases for path A1, as the dopant is positioned closer to the outer sites. This is particularly interesting because the {100} surfaces do not delaminate,[33] and although no inner surface exists along these paths, the energy of boron atoms along these paths show evidence of sensitivity to the core−shell structure of the particle as a whole. In contrast, paths B, D, and E all cross the inner surface of the core (intersecting directly with the core−shell structure of the bucky-diamond), but with slightly different results. Note that, along paths D and E (toward the {111}/{111} edge and {100}/{111}/{111} corner, respectively), there is a decrease (of ∼0.5 eV) in energy at the sites just below the inner surface of the core compared to the sites located *on* the inner surfaces. This type of feature is reproduced at the outer sites (in all but path A1), where in the shell of the bucky-diamond, the boron dopants occupying subsurface sites are lower in energy than those positioned at the actual extremum. In general, the subsurface site for path D (just below the {111}/{111} edge) is the lowest-energy position for a boron dopant in the bucky-diamond particle (although the energy difference is very slight).

We can see from Figure 4b that boron substitution in bucky-diamond is relatively insensitive to the local crystallographic structure of the extremum (with surfaces, edges, and corners being energetically very similar). Also, with the exception of the inner surface along path B and the extremum of path A1, there is a general trend that subsurface (subedge or subcorner) sites are energetically preferred positions for boron substitution than actual surfaces, edges, or corners. This result is interesting because we have previously found the opposite is true for nitrogen substitution in bucky-diamond (nitrogen atoms preferring the extremal sites rather than the subextremal sites), as reported in ref 20.

**3.3. Nanodiamond.** In the case of the cubic nanodiamond particle, the boron atoms were found once again to prefer 4-fold coordination within the core region, irrespective of location. At the outer sites of path A2 and path I, the boron atoms were also found to be stable in the (natural) undercoordinated sites (showing only the expected outward relaxation), however, in paths F, G, and H, this was not the case. The effect of boron substitution near {110} surfaces (path F), {100}/{110} edges (path G), and {110}/{110} edges (path H) was found to be quite

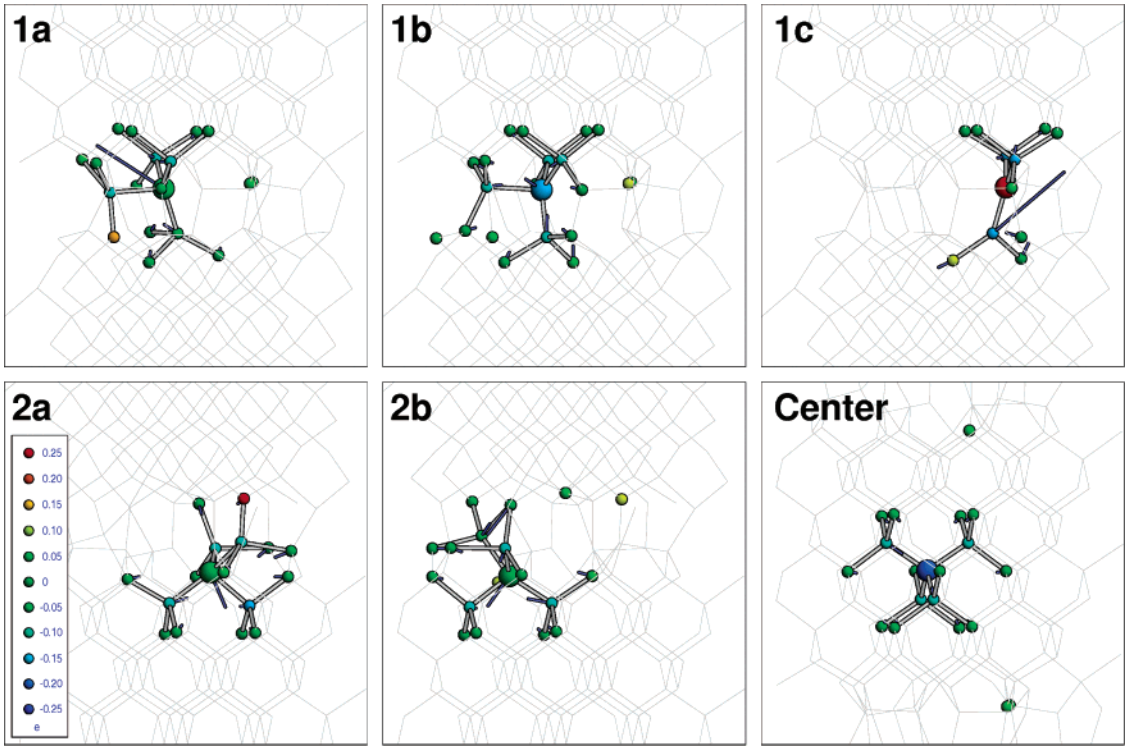


**Figure 6.** Atomic structure of the nanocrystalline diamond thin film with boron substitutions at each unique grain boundary site and at the center of the grain. The boron atoms are indicated by a larger sphere. Also shown are significant changes in atomic Mulliken charges ($\Delta c = c_B - c_{diam}$), indicated by a color scale, when $|\Delta c| > 0.04$. Also shown are changes in position of these atoms resulting from the re-relaxation of the B atom and surrounding neighbors ($\Delta \mathbf{R} = \mathbf{R}_{diam} - \mathbf{R}_B$), shown as 10-fold scaled vectors in blue.

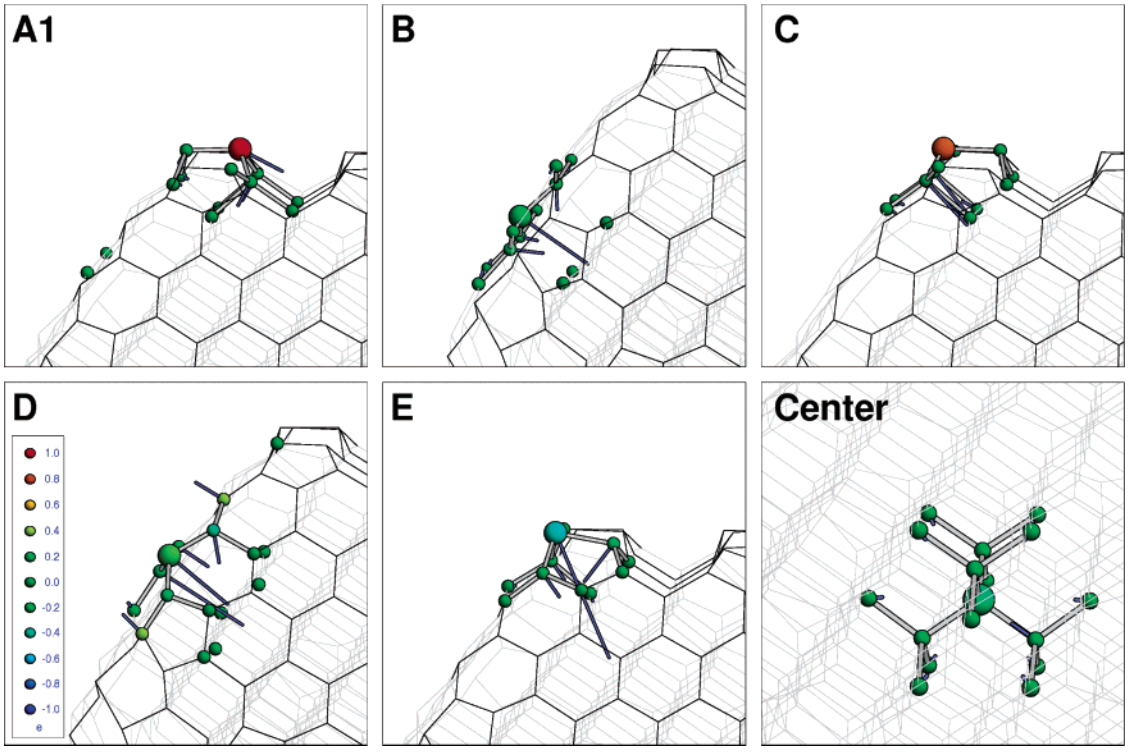


**Figure 7.** Atomic structure of the bucky-diamond, with boron substitutions at the extremum for each substitution path (indicated in the top left corner of each image) and at the centrosymmetric site. The boron atoms are indicated by a larger sphere. Significant changes in atomic Mulliken charges and changes in position of these atoms resulting from the re-relaxation of the B atom and surrounding neighbors are shown as described for Figure 6.

disruptive. Boron dopants located at extremum sites (as well as subsurface and, in some cases, sub-subsurface sites) broke bonds with neighboring carbon atoms and adopted 3-fold, 2-fold, or even 1-fold coordinated configurations.

Energetically, however, boron substitution into (or bordering) a {110} surface appears less unfavorable than would be expected given the structural changes. In a fashion similar to the results for the bucky-diamond described above in Section 3.2, in the

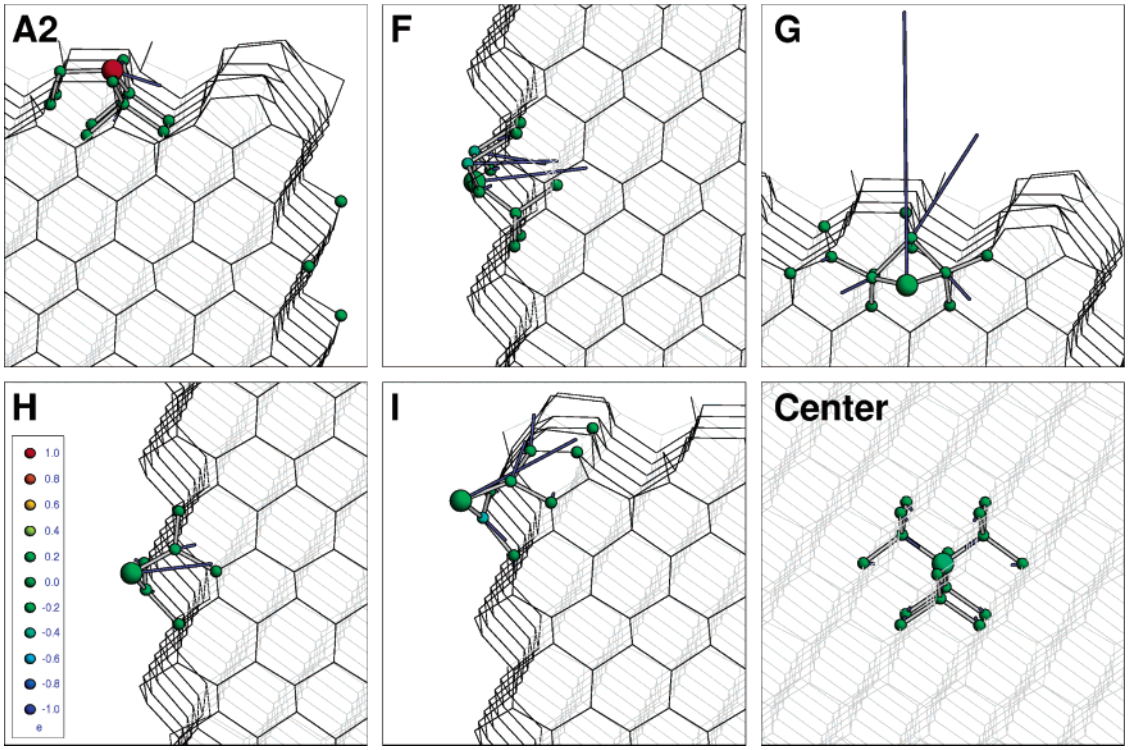


**Figure 8.** Atomic structure of the nanodiamond particles, with boron substitutions at the extremum for each substitution path (indicated in the top left corner of each image) and at the centrosymmetric site. The boron atoms are indicated by a larger sphere. Significant changes in atomic Mulliken charges and changes in position of these atoms resulting from the re-relaxation of the B atom and surrounding neighbors are shown as described for Figure 6.

core region (less than $r/R \approx 0.5$ in Figure 4c), the results are insensitive to the substitution path,[32] with differences emerging beyond this region. Over $r/R \approx 0.6$, the energy for boron substitution along paths F, G, and H decreases, with paths G and H showing a rapid decrease in energy until the substitution site is located at the extremum. In contrast, there is an increase in energy for sites along path A2 and path I (which were the sites showing the least structural disruption), resulting in an endothermal maximum again for boron substitution within the range $r/R \approx 0.8-1$. The extremum of path I is ~3 eV lower in energy than the extremum of path A2, the former being located at a particle corner and the latter being a site that participates in a $(2 \times 1)$ dimer near the center of the facet.

In general, the substitution site located at the extremum of path G (on the {110}/{110} edge) is the lowest-energy position for a boron atom in the cubic nanodiamond particle (and the lowest overall). A boron atom at this site is 5.5 eV lower in energy than if located at the center of the particle, as shown in Figure 4c. Overall, the results here indicate that boron substitution is more (energetically) favorable on a site bordering (but not located directly on) a {110} surface facet than others considered in this study.

**3.4. Influence of Particle Shape.** As mentioned above, an advantage of the choice of structures used in this study is that an investigation of the effect of the nanoparticle shape upon the results can be made because substitution paths along the ⟨100⟩ direction were investigated for both the bucky-diamond and nanodiamond particles (paths A1 and A2, respectively). Recall that, even in the bucky-diamond, no surface delamination occurs on this surface, and both facets exhibited the $(2 \times 1)$ surface reconstruction. The results for path A1 and A2 are shown together in Figure 5, where we can see some remarkable differences. Below $r/R \approx 0.4$, the shape of the particle has no impact on the energy for boron substitution, but beyond this (core) region, two main shape-dependent differences are evident. The first is that, in the (radial) region between $r/R \approx 0.6$ and 0.8, the results for bucky-diamond are exothermal (showing a decrease in energy for boron substitution), whereas the results for nanodiamond are endothermal (showing an increase in energy for boron substitution). The second difference is at the extremum ($r/R = 1$), where the energy for boron substitution is lower for the bucky-diamond than that for the nanodiamond, even though both sites participate in a $(2 \times 1)$ surface dimer located at the center of the facets. On the basis of these findings, the relationship between particle shape and the substitution energy of dopants or impurities is the topic of further investigation.

**3.5. Distribution of Charge at Preferred Sites.** Table 1 indicates the net atomic Mulliken charges of the original carbon site, the boron substituent after substitution, and their difference, defined as $\Delta c = c_B - c_{diam}$. Figures 6−8 illustrate these results for atoms in the vicinity of the dopant where $|\Delta c| > 0.04$.

Within the GB, all charge redistributions are within ±0.25, whereas for the cluster models, we observe values reaching 1.0 for the surface dimer sites. Aside from those large values for boron atoms, other atoms with changes above the cutoff correlate with the relaxation restriction to second neighbors. There are a few exceptional cases where farther atoms at adjacent surfaces and within the GB show a change above the cutoff.

As noted, the largest changes occur for sites participating in (100) surface dimers, which are A1, A2, C, and E. In the original carbon decoration, these sites hold occupied dangling bonds, but are neutral after boron substitution. The first three sites are quite similar in structure before and after substitution (with displacements up to 0.15 Å). This is reflected in similar charges. The exception is the corner site E, which undergoes a relatively large outward relaxation, which results in a fully occupied dangling bond on the boron atom. The center sites for all three structures (GB, bucky-diamond, and nanodiamond) are also structurally and thus electronically similar. With carbon decora-

tion, they are all neutral (as expected) and slightly negative (−0.2 to −0.3) after substitution. Overall, in contrast to the nitrogen substitution from our previous work,[20] we cannot identify a correlation between the Mulliken charges and the substitution energy for boron substitution.

## 4. Conclusion

Presented here are density functional tight-binding simulations examining the configuration, potential energy surface, and electronic charge of substitutional boron in various types of nanocrystalline diamond. The present study has also been designed to complement our previous work on the structure and stability of nitrogen in nanodiamond and bucky-diamond particles. The results predict that boron is likely to be positioned at the extremum of isolated particles and at the grain boundary (GB) of thin-film samples.

For sites in the immediate GB layer and its adjacent monolayer, the energy is 2−2.5 eV lower than that at the center, clearly indicating that boron is likely to be preferentially located near or in the grain boundaries. In the case of bucky-diamond, it was found that subsurface (subedge or subcorner) sites are energetically preferred sites for boron substitution than extremum sites at surfaces, edges, or corners. The subsurface site just below the {111}/{111} edge was found to be the lowest-energy position for a boron atom, although the energy difference with other subsurface sites was only very slight. This result is in contrast to previous results for nitrogen substitution in bucky-diamond (nitrogen atoms preferring the extremal sites rather than the subextremal sites)[20] and was inconsistent with results for the cubic nanodiamond particle. In the latter case, a subsurface site was only found to be preferable beneath a {110} surface facet, with all other extremum being lower in energy than their subsurface counterparts. From these results, we have identified evidence of shape dependence that will form the basis of future work.

**Acknowledgment.** This work has been supported by the Glasstone Benefaction at the University of Oxford, and the U.S. Department of Energy, Basic Energy Sciences, under contract W-31-109-ENG-38.

## References and Notes

(1) Gheeraert, E.; Koizumi, S.; Teraji, T.; Kanda, H.; Nesladek, M. *Phys. Status Solidi A* **1999**, *174*, 39.

(2) Kalish, R. *Carbon* **1999**, *37*, 781.

(3) Popovici, G.; Wilson, R. G.; Sung, T.; Prelas, M. A.; Khasawinah, S. *J. Appl. Phys.* **1995**, *70*, 5103.

(4) Sattel, S.; Robertson, J.; Tass, Z.; Scheib, M.; Wiescher, D.; Ehrhardt, H. *Diamond Relat. Mater.* **1997**, *6*, 255.

(5) Gruen, D. M. *Annu. Rev. Mater. Sci.* **1999**, *29*, 211.

(6) Proffitt, S. S.; Probert, S. J.; Whitfield, M. D.; Foord, J. S.; Jackman, R. B. *Diamond Relat. Mater.* **1999**, *8*, 768.

(7) Sharda, T.; Soga, T.; Jimbo, T.; Umeno, M. *Diamond Relat. Mater.* **2001**, *10*, 1592.

(8) Sharda, T.; Soga, T. *J. Nanosci. Nanotechnol.* **2003**, *3*, 521.

(9) Wang, T.; Xin, H. W.; Zhang, Z. M.; Dai, Y. B.; Shen, H. S. *Diamond Relat. Mater.* **2004**, *13*, 6.

(10) Loubnin, E. N. *J. Vac. Sci. Technol., B* **2004**, *22*, 1319.

(11) Yater, J. E.; Shih, A.; Butler, J. E.; Pehrsson, P. E. *J. Appl. Phys.* **2003**, *93*, 3082.

(12) Yater, J. E.; Shih, A.; Butler, J. E.; Pehrsson, P. E. *J. Appl. Phys.* **2004**, *96*, 446.

(13) Muna, G. W.; Tasheva N.; Swain, G. M. *Environ. Sci. Technol.* **2004**, *38*, 3674.

(14) Show, Y.; Witek, M. A.; Sonthalia, P.; Swain, G. M. *Chem. Mater.* **2003**, *15*, 879.

(15) Lee, Y.-C.; Lin, S.-J.; Lin, I.-N.; Cheng, H.-F. *J. Appl. Phys.* **2005**, *97*, 054310.

(16) Cheng, H.-F.; Lee, Y.-C.; Lin, S.-J.; Chou, Y.-P.; Chen, T. T.; Lin, I.-N. *J. Appl. Phys.* **2005**, *97*, 044312.

(17) Park, S.; Srivastava, D.; Cho, K. *J. Nanosci. Nanotechnol.* **2001**, *1*, 75.

(18) Porezag, D.; Frauenheim, Th.; Köhler, Th.; Seifert, G.; Kaschner, R. *Phys. Rev. B* **1995**, *51*, 12947.

(19) Frauenheim, Th.; Seifert, G.; Elstner, M.; Niehaus, Th.; Köhler, C.; Amkreutz, M.; Sternberg, M.; Hajnal, Z.; Di Carlo, A.; Suhai, S. *J. Phys.: Condens. Matter* **2002**, *14*, 3015.

(20) Sternberg, M.; Horner, D. A.; Redfern, P. C.; Zapol, P.; Curtiss, L. A. *J. Comput. Theor. Nanosci.* **2005**, *2*, 207.

(21) Barnard, A. S.; Sternberg, M. *J. Phys. Chem. B* **2005** *109*, 105.

(22) Zapol, P.; Sternberg, M.; Curtiss, L. A.; Frauenhiem T.; Gruen, D. M. *Phys. Rev. B* **2001**, *65*, 045403.

(23) Barnard, A. S.; Russo, S. P.; Snook, I. K. *J. Chem. Phys.* **2003**, *118*, 5094.

(24) Barnard, A. S.; Russo, S. P.; Snook, I. K. *Phys. Rev. B* **2003**, *68*, 073406.

(25) Barnard, A. S.; Russo, S. P.; Snook, I. K. *Diamond Relat. Mater.* **2003**, *12*, 1867.

(26) Russo, S. P.; Barnard, A. S.; Snook, I. K. *Surf. Rev. Lett.* **2003**, *10*, 233.

(27) Although the present study is not a diffusion or migratory study, it is clear that this represents a potential energy barrier that may prevent boron from diffusing to the surface in this direction.

(28) Barnard, A. S.; Russo, S. P.; Snook, I. K. *Philos. Mag. B* **2003**, *83*, 1163.

(29) Goss, J. P.; Briddon, P. R. *Phys. Rev. B* **2006**, *73*, 085204.

(30) Goss, J. P.; Briddon, P. R.; Jones, R.; Teukam, Z.; Ballutaud, D.; Jomard, F.; Chevallier, J.; Bernard, M.; Deneuville, A. *Phys. Rev. B* **2003**, *68*, 235209.

(31) Lombardi, E. B.; Mainwood, A.; Osuch, K. *Phys. Rev. B* **2004**, *70*, 205201.

(32) Breuer, S.; Briddon, P R. *Phys. Rev. B* **1994**, *49*, 332.

(33) Between $r/R = 0.3$ and ∼0.5, although small energetic differences between the substitution paths may be discerned, these differences are less than the uncertainty introduced by using the second-nearest neighbor approximation, as described in ref 20.

(34) Kuznetsov, V. L.; Zilberberg, I. L.; Butenko, Y. V.; Chuvilin, A. L.; Seagall, B. *J. Appl. Phys.* **1999**, *86*, 863.